Discharge, discharge variability, and the bedrock channel profile

Dimitri Lague[1] and Niels Hovius

Department of Earth Sciences, University of Cambridge, Cambridge, UK

Philippe Davy

Géosciences Rennes, UMR 6118, CNRS, Université de Rennes I, Rennes, France

[1] Long-term bedrock incision is driven by daily discharge events of variable magnitude and frequency, with ineffective events below an incision threshold. We explore theoretically how this short-term stochastic behavior controls long-term steady state incision rates and bedrock channel profiles, combining a realistic frequency-magnitude distribution of discharge with a deterministic, detachment-limited incision model in which incision rate is a power function of basal shear stress above a critical shear stress. Our model predicts a power law relationship between steady state slope and drainage area consistent with observations. The exponent of this power law is independent of discharge mean and variability, while the amplitude factor, which controls mountain belt relief, is a power law function of mean runoff (with an exponent of −0.5) and a complex function of runoff variability. In accordance with evidence that incision occurs between 6 and 20% of time in rapidly incising rivers (>1 mm/yr) our model predicts that channel steepness is virtually insensitive to runoff variability. Runoff variability can only decrease channel steepness for very slow incision rates and/or weak lithologies. The relationship between channel steepness and incision rate is always a power law whose exponent depends on the channel cross-sectional geometry and runoff variability. This contradicts models neglecting discharge stochasticity in which the steepness-incision scaling is set by the incision law exponent. Our results suggest that changes in climate variability cannot explain an increase in bedrock incision rates during the Late Cenozoic within the context of a detachment limited model.

1. Motivation

[2] Changes in global climate affect the mean water discharge in rivers, and its temporal distribution between rare extreme events (floods and droughts) and frequent normal events [*Ely*, 1997]. This is likely to have an impact on long-term river incision [*Molnar*, 2001; *Tucker and Bras*, 2000; *Tucker and Slingerland*, 1997] and landscape lowering. Climate-driven changes in erosion modify the flux of sediment to depositional basins [*Clift et al.*, 2002; *Harris and Mix*, 2002; *Zhang et al.*, 2001], the weathering drawdown of atmospheric CO_2 [*Millot et al.*, 2002] and the sequestration of organic carbon [*France-Lanord and Derry*, 1997], with feedbacks to global climate [*Raymo and Ruddiman*, 1992; *Ruddiman and Preil*, 1997]. These changes also govern landscape morphology at local [*Rinaldo et al.*, 1995; *Tucker and Bras*, 2000; *Tucker and Slingerland*, 1997; *Whipple et al.*, 1999] and continental

scales, and can potentially change exhumation and tectonic deformation of mountain belts [*Hilley and Strecker*, 2004; *Molnar and England*, 1990; *Whipple and Meade*, 2004]. Progress in our understanding of the feedbacks between atmospheric and lithospheric processes, as well as the stratigraphic signature of past climate changes critically depends on our quantitative understanding of the role of discharge and discharge variability in continental erosion.

[3] Bedrock rivers are central to this problem. They incise the substrate, drive mass wasting, and remove the erosion products. Many studies have modeled the dynamics and geometry of bedrock river channels with incision laws assuming a simple relation between the rate of vertical incision, channel slope and discharge [*Braun and Sambridge*, 1997; *Crave and Davy*, 2001; *Howard*, 1994; *Kooi and Beaumont*, 1996; *Lague et al.*, 2000; *Tucker and Slingerland*, 1994; *Willgoose et al.*, 1991]. In these studies, fluvial incision is commonly scaled with the mean annual discharge or an effective discharge with a given recurrence time, and these parameters are thought to reflect the long-term integration of discharges of different magnitude and frequency. This approach would be valid if, for example, the effective discharge were identical for all incision rates and/or

---

[1]Now at Géosciences Rennes, UMR 6118, CNRS, Rennes, France.

discharge probability distributions. However, this is unlikely when the chosen incision law is nonlinear with respect to discharge, and climate change is characterized by shifts in the relative frequencies of large and small events. This problem has been addressed by using simplified frequency-magnitude distributions of discharge [*Molnar*, 2001; *Snyder et al.*, 2003b; *Tucker*, 2004; *Tucker and Bras*, 2000], and it has emerged that the constant effective discharge model is indeed inappropriate when the threshold of erosion is nonnegligible. Then, its application would result, for example, in an erroneous prediction of the scaling of channel slope with rock uplift rate. Various authors have independently argued that thresholds of detachment or entrainment cannot be neglected [*Lague et al.*, 2003; *Lague and Davy*, 2003; *Snyder et al.*, 2003b; *Tucker*, 2004] and that these thresholds have a profound impact on landscape geometry and dynamics [*Baldwin et al.*, 2003; *Lague et al.*, 2003; *Molnar*, 2001; *Tucker*, 2004]. If correct, these findings compel a fuller investigation of the impact of discharge variability on longitudinal channel geometry.

[4] Building on the work by *Snyder et al.* [2003b], *Tucker and Bras* [2000], and *Tucker* [2004], we use a realistic, stochastic distribution of daily discharge coupled with a deterministic incision law to derive approximate analytical solutions that predict the theoretical scaling between channel slope, drainage area, long-term incision rate and discharge characteristics (mean and variability) at steady state. We focus on detachment-limited models in which channel dynamics are set by the rate of bedrock incision. This rate is a power function of the basal shear stress, above a critical value required to entrain bed load or detach bedrock [*Howard*, 1994; *Howard and Kerby*, 1983]. This choice is justified by the finding that incision proportional to basal shear stress can reasonably predict incision rates in rapidly cutting rivers [*Lavé and Avouac*, 2001]. Moreover, it remains to date the most widely used model of mountain channel evolution [*Finlayson et al.*, 2002; *Howard*, 1994; *Roe et al.*, 2003; *Snyder et al.*, 2003b; *Sobel et al.*, 2003; *Whipple and Meade*, 2004], and as such deserves a thorough study of the importance of runoff variability. We do not restrict our study to a particular set of incision law parameters, but rather explore predictions for various parameter combinations.

[5] We start by introducing the stochastic model of daily discharge, the incision law and the derivation of the long-term incision rate. Then, we calculate the steady state channel slope-drainage area relationship and its dependency with (1) the nonlinearity of the incision law (possibly reflecting the type of bedrock incision process [*Whipple et al.*, 2000]), (2) the value of the critical shear stress, (3) the cross-sectional geometry of the channel (the principle control on the variation of flow width with discharge), and (4) the incision rate, mean runoff, and runoff variability. Finally, we explore the relative importance of mean runoff and runoff variability in setting the steady state geometry of bedrock channels.

2. Runoff Distribution and Incision Law

2.1. Frequency-Magnitude Distribution of Discharge

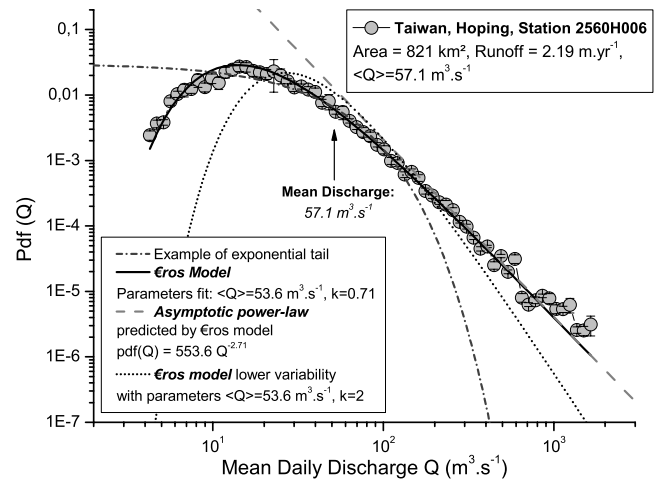[6] Rivers have a natural variability of discharges at daily timescale, with rare extremes (droughts and floods) punc-

Figure 1. Frequency-magnitude distribution of daily discharge for 30 years of records in the Hoping River of Taiwan (data publicly available from http://gweb.wra. gov.tw/wrweb/) and calculated using the averaging method of *Davy* [1993]. Examples of (1) exponential distribution as used by *Tucker and Bras* [2000], (2) best fit for the €ros distribution model used in this study (least squares regression weighted by errors bars) [*Crave and Davy*, 2001], and (3) asymptotic power law distribution of flood as used by *Molnar* [2001] are also shown. Another €ros distribution with the same mean discharge but a variability parameter $k = 3$ is shown, illustrating the fact that as k increases, the probability of extreme events (large and small) decreases compared to frequent events. See color version of this figure in the HTML.

tuating common flow conditions. Discharge fluctuations are mainly due to variability of precipitation, and filtered by (climate-governed) watershed processes such as evapotranspiration, infiltration, and snow accumulation and melt. The variability of river discharge at a given location can be characterized by the frequency-magnitude distribution of mean daily discharge (Figure 1). This distribution generally consists of two trends: (1) at low flow, the frequency of a given event increases with discharge (meaning that droughts are relatively rare), and (2) at intermediate and high flow, the frequency of events decreases with increasing discharge (Figure 1). Most importantly, the probability distribution of large floods can often be fit with a power law [*Turcotte and Greene*, 1993]. In an analysis of 20 gauging stations in the United States, the power law exponent was found to vary between −2.1 and −4.3 [*Turcotte and Greene*, 1993] (Figure 1). Note that the frequency of extreme floods decreases with the absolute value of the exponent.

[7] Previous work on the impact of discharge variability on channel erosion has used stochastic models of rainfall with simplified catchment hydrology [*Snyder et al.*, 2003b; *Tucker*, 2004; *Tucker and Bras*, 2000; *Tucker and Slingerland*, 1997], or stochastic models of discharge [*Crave and Davy*, 2001; *Molnar*, 2001]. For example, pioneering work by *Tucker and Bras* [2000] was based on a Poisson pulse rainfall model coupled with a simple Hortonian and uniform runoff assumption for which the probability distribution of finite discharges has an exponential distribution. This is not consistent with the observed power law tailing of

discharge distributions, and causes underestimation of the frequency of extreme events (Figure 1). Moreover, the rainfall intensity probability distribution of convective precipitation systems, for which the rainfall variability is largest, tends to display power law rather than exponential tailing [*Olsson and Burlando*, 2002; *Svensson et al.*, 1996]. In agreement with this, *Molnar* [2001] used a simple power law frequency-magnitude distribution of discharges, but neglected the rollover at low flow, arguing that incision (and sediment transport) only occurs at very large discharges for which power law scaling is dominant. This assumption bars the evaluation of cases for which the erosion threshold is negligible or small and outside the power law domain.

[8] We use the two-parameter frequency-magnitude distribution of daily discharge events of the landscape evolution model €ros [*Crave and Davy*, 2001; *Davy and Crave*, 2000]. This simple model overcomes the limitations of previous studies. The probability density function of daily discharge Q is given by (Figure 1)

$$pdf_{\bar{Q},k}(Q) = \frac{(\bar{Q}k)^{k+1}}{\Gamma(k+1)} \exp\left(-k\frac{\bar{Q}}{Q}\right) Q^{-(2+k)} dQ, \quad (1)$$

where $\bar{Q}$ is the mean discharge and k is a parameter setting the discharge variability (note that the variability is greatest for small values of k) (Figure 1)). The gamma function $\Gamma(k+1)$ equals $k!$ when k is an integer. It is useful to normalize discharge:

$$Q^* = Q/\bar{Q}. \quad (2)$$

The normalized discharge is independent of drainage area, provided that mean runoff $\bar{R}$ is spatially uniform. Using equation (2), equation (1) becomes

$$pdf_{\bar{Q},k}(Q^*) = \frac{k^{k+1}}{\Gamma(k+1)} \exp\left(-\frac{k}{Q^*}\right) Q^{*-(2+k)} dQ^*. \quad (3)$$

Equation (3) has two main components (Figure 1): (1) an inverse exponential tail that represents the lesser probability of very small discharges compared to the most probable daily discharge and (2) an asymptotic power law tail for floods (with an exponent $-(2 + k)$), consistent with observations by *Turcotte and Greene* [1993]. Figure 1 shows that this model fits the two trends observed in daily discharge data from the Hoping river in Taiwan, especially the asymptotic power law distribution. To validate the discharge model, we have analyzed long time series ($\leq$30 yr) of daily discharge measurements from 22 hydrometric stations in Taiwan (http://gweb.wra.gov.tw/wrweb/) and 8 in the United States [*Slack et al.*, 1993]. We found that the variability parameter k is between 0.08 and 1.1 in Taiwan, and between 0.9 and 1.85 in the United States [*Slack et al.*, 1993]. This is consistent with values of 0.1–2.23 obtained by Turcotte and Greene using a power law model to fit the distribution of maximal annual floods in the U.S. Using published values of the ratio between the median daily discharge and the mean annual discharge (which uniquely depends on k), for 59 hydrometric stations around the world with at least 3 years of records [*Meybeck et al.*, 2003], yields estimates of k from 0.15 to 3, with most

values around 1. Here, we assume that the present-day range of k is from 0.1 to 3. Quantitative estimates of the discharge variability of past climates are not available, and we assume that the range of k values has not changed with time.

[9] For a discharge distribution of parameters $\bar{Q}$ and k, a convenient measure of the probability of occurrence of a given discharge Q_c^* is its return time $t_r(Q_c^*)$:

$$t_r(Q_c^*) = P(Q^* \geq Q_c^*)^{-1}. \quad (4)$$

where $P(Q^* \geq Q_c^*)$ is the probability that Q^* is greater than Q_c^*. Using, equation (3), $P(Q^* \geq Q_c^*)$ is equal to

$$P(Q^* \geq Q_c^*) = \int_{Q_c^*}^{+\infty} pdf_{\bar{Q},k}(Q^*) dQ^* = \Gamma(k/Q_c^*, k+1) \quad (5)$$

where $\Gamma(x, a)$ is the incomplete Gamma function $\Gamma(x, a) = \frac{1}{\Gamma(a)} \int_0^x y^{a-1} e^{-y} dy$, increasing from 0 to 1 with x, for any $a > 0$. Hence the return time of discharge Q_c^*, for any combination of k and $\bar{Q}$ is equal to

$$t_r(Q_c^*) = \Gamma(k/Q_c^*, k+1)^{-1} \quad (6)$$

2.2. Instantaneous Incision Law

[10] The incision of rivers into bedrock results from the summation of elementary wear events, typically lasting hours to days, over thousands of year. Many incision laws have been devised empirically to be effective at geological timescales: they do not necessarily work at hydrological timescales [*Beaumont et al.*, 1992; *Braun and Sambridge*, 1997]. In contrast, recent mechanistic models [*Sklar and Dietrich*, 2004] are defined at short timescales, and their upscaled formulation at geological timescales remains to be determined. Our goal is to proceed in that direction, by studying the long-term predictions obtained from the stream power family of bedrock incision models applied at daily timescales. The stream power model was first formulated by *Howard and Kerby* [1983]. It has been used in a large number of studies [*Finlayson et al.*, 2002; *Howard*, 1994; *Lavé and Avouac*, 2001; *Seidl and Dietrich*, 1992; *Snyder et al.*, 2000; *Sobel et al.*, 2003; *Stock and Montgomery*, 1999; *Tucker and Bras*, 2000; *Tucker and Slingerland*, 1994; *Whipple*, 2001; *Whipple and Meade*, 2004; *Whipple and Tucker*, 1999]. Empirically, it is written as [*Howard and Kerby*, 1983]

$$I = k_e(\tau - \tau_c)^a, \quad \tau > \tau_c, \quad (7)$$

where I is the vertical incision rate, k_e is an erosion efficiency coefficient, a is an exponent expected to be dependent on the principal incision process [*Whipple et al.*, 2000], τ is the basal shear stress and τ_c is a critical shear stress above which incision starts. Given the uncertainty on the formulation of the incision rate, we use a modified version [*Baldwin et al.*, 2003; *Snyder et al.*, 2003b; *Tucker*, 2004] for ease

$$I = k_e(\tau^a - \tau_c^a), \quad \tau > \tau_c. \quad (8)$$

Note that equations (7) and (8) differ significantly in their prediction of the incision rate when τ is close to τ_c and $a > 1$.

[11] The hydraulics of bedrock channels are poorly understood and the applicability of empirical flow resistance equations such as Manning or Darcy-Weisbach used for alluvial rivers has not been systematically checked. As a consequence, the calculation of basal shear stress as a function of discharge remains empirical. We choose to follow the derivation commonly used in channel incision studies [Howard, 1994; Tucker and Bras, 2000; Whipple et al., 1999], assuming steady uniform flow in a wide channel (for which the hydraulic radius can be approximated by flow depth), and using resistance equations such as Manning or Darcy-Weisbach to express basal shear stress as a function of channel bed gradient S (taken, for small values, as the tangent of the angle of the channel bed with the horizontal), water discharge, and flow width w:

$$\tau = k_t \left(\frac{Q}{w}\right)^\alpha S^\beta, \qquad (9)$$

where k_t is an hydraulic factor encompassing water density, gravity acceleration and a friction factor. Parameters α and β are equal to 3/5, and 7/10 for Manning, and 2/3, and 2/3 for Darcy-Weisbach (see Howard [1994] for a complete derivation).

[12] As shown in equation (9) the variation of flow width with discharge at a given location (which is a characteristic of the at-a-station hydraulic geometry of channels [Leopold and Maddock, 1953]) partly controls the scaling of basal shear stress with discharge. The smaller is the variation of flow width with discharge, the larger is the increase of shear stress (and incision rate) with discharge. A rectangular channel cross section gives the greatest shear stress rise for a given discharge increase. In alluvial rivers, the relationship between flow width and discharge tends to have the form of a power law [Leopold and Maddock, 1953] with an exponent ranging from 0.04 to 0.26 [Knighton, 1998]. This exponent is largely controlled by the channel cross-section geometry, and modulated by changes in the flow resistance of the channel bed and walls with discharge. In the absence of empirical data for bedrock channels, we use the same power law model. This is convenient because it allows for representation of a range of cross-sectional shapes, including a rectangle, simply by varying the exponent. We assume that the variation of flow width with discharge is no greater in bedrock channels than in alluvial channels (this is reasonable because the flow is always contained within valley walls). Hence we consider values of the exponent between 0 and 0.25.

[13] In uniform lithological and tectonic settings, the mean channel width increases downstream with discharge [Leopold and Maddock, 1953; Montgomery and Gran, 2001; Snyder et al., 2003a] according to a power law. In alluvial rivers, bank-full discharge is generally used as a reference flow for measurement of channel width. Bedrock channels are contained between valley walls that make the definition of a bank-full width difficult. Therefore we define the local channel width as the flow width w_a at mean discharge $\bar{Q}$:

$$w_a = k_w \bar{Q}^{\omega_a}, \qquad (10)$$

where k_w is an amplitude factor depending on lithology, incision rate, and, arguably, discharge variability, and ω_a is a scaling exponent pertaining to the downstream variation of flow width. The local, at-a-station variation of flow width w with discharge is described as a function of w_a:

$$\frac{w}{w_a} = \left(\frac{Q}{\bar{Q}}\right)^{\omega_s}, \qquad (11)$$

where ω_s is a scaling exponent reflecting the temporal variations of local flow width. Combining equations (8), (9) and (2) gives the following general expression of flow width:

$$w = k_w Q^{*\omega_s} \bar{Q}^{\omega_a}. \qquad (12)$$

Substitution of equations (9) and (12) in equation (8) then gives a "daily" incision law whose general expression is

$$I(\bar{Q}, Q, S) = K \bar{Q}^m Q^{*\gamma} S^n - \psi_c \qquad (13)$$

with, $K = k_e k_t^a k_w^{-a\alpha}$, $m = a\alpha(1 - \omega_a)$ the downstream discharge exponent, $\gamma = a\alpha(1 - \omega_s)$ the local discharge exponent, and $n = a\beta$ the slope exponent. We define the threshold parameter ψ_c as

$$\psi_c = k_e \tau_c^a. \qquad (14)$$

[14] The daily incision law in equation (13) resembles the traditionally used stream power incision law with threshold (for example, the expressions of m and n are the same [see Whipple and Tucker, 1999]), except for the daily discharge term raised to the power γ. The two would be equal in the case $\omega_s = \omega_a$, for which equation (13) transforms into

$$I = K Q^m S^n - \psi_c. \qquad (15)$$

However ω_s (0–0.25) is generally smaller than ω_a (~0.5), and this causes m to be smaller than γ (Table 1). As γ captures the impact of discharge variability on long-term incision, it is clear that the "long-term" form of the stream power incision law shown in equation (15) does not permit investigation of the impact of discharge variability: the exponent m does not fully represent the degree of nonlinearity of incision rate with daily discharge. For example, m is predicted to range from 0.3 to 0.83, depending on the incision model (Table 1), γ spans a wider range from 0.45 to 1.67. In the simple case of a negligible incision threshold and for $a = 5/2$, equation (13) would predict an important impact of large and infrequent events on long-term incision, while frequent, small events would dominate the long-term incision rate according to equation (15). In the next section, we explore the impact of γ on the contribution of large events to long-term fluvial incision in more detail.

2.3. Long-Term Incision Rate

[15] The mean long-term incision rate $\bar{I}$ is obtained by integrating the action of all erosive discharge events

Table 1. Values of Parameters γ, m, and n for Various Incision Laws, Channel Cross-Sectional Geometry, and Flow Resistance Equation[a]

Shear Stress Exponent a	Theoretical Model and Example of Field Evidence (If Any)	Local Discharge Exponent γ				Downstream Discharge Exponent m		Slope Exponent n	
		$\omega_s = 0$: Rectangular Cross Section		$\omega_s = 0.25$: Concave Cross Section					
		M	DW	M	DW	M	DW	M	DW
1	shear stress model[b,c]	0.6	0.67	0.45	0.5	0.3	0.33	0.67	0.7
3/2	unit stream power, plucking[d]	0.9	1	0.67	0.75	0.45	0.5	1	1.05
5/2	suspended load abrasion[d]	1.5	1.67	1.13	1.25	0.75	0.83	1.67	1.75

[a]DW, Darcy-Weisbach; M, Manning; $\omega_a = 0.5$.
[b]*Howard and Kerby* [1983].
[c]*Lavé and Avouac* [2001].
[d]*Whipple et al.* [2000].

given by equation (13) weighted by their probability of occurrence:

$$\bar{I} = \int_{Q_c^*}^{Q_m^*} I(\bar{Q}, Q^*, S)\, pdf_{\bar{Q},k}(Q^*)\, dQ^*, \qquad (16)$$

where Q_c^* is the minimum discharge for which the critical shear stress τ_c in equation (8) is overcome and Q_m^* is the maximum discharge at the timescale considered – this is statistically equal to the return time of Q_m^*. We solve this integral assuming that the 3D geometry of the channel (cross section and longitudinal slope), the parameters of the incision law and the parameters of the frequency-magnitude distribution of discharge are stationary over $t_r(Q_m^*)$. Introducing equation (13) and (3) in equation (16) and solving gives

$$\bar{I} = K \frac{\Gamma(k+1-\gamma)k^{\gamma}}{\Gamma(k+1)} \left[\Gamma\left(k/Q_c^*, k+1-\gamma\right) \right.$$
$$\left. - \Gamma\left(k/Q_m^*, k+1-\gamma\right) \right] \bar{Q}^m S^n \qquad \text{, for } \gamma < k+1 \quad (17)$$
$$- \left[\Gamma\left(k/Q_c^*, k+1\right) - \Gamma\left(k/Q_m^*, k+1\right) \right] \psi_c$$

[16] In the case of a negligible threshold, and infinite maximum discharge Q_m^* (though we always expect a physical discharge limit even for infinite time), the long-term incision rate (here termed the reference incision rate $\bar{I}^{ref}$) is equal to

$$\bar{I}^{ref} = K \frac{\Gamma(k+1-\gamma)k^{\gamma}}{\Gamma(k+1)} \bar{Q}^m S^n. \qquad (18)$$

Equation (18) is close to the general form of the stream power incision law [*Seidl and Dietrich*, 1992; *Snyder et al.*, 2000; *Stock and Montgomery*, 1999; *Tucker and Slingerland*, 1994; *Whipple and Meade*, 2004; *Whipple and Tucker*, 1999] except for the explicit formulation of the role of discharge variability. It shows that the downstream discharge exponent m sets the dependency of incision rate on mean discharge, while its dependency on discharge variability is a complex function of k and γ (set by the incision law and the local hydraulic geometry). The variation of $\bar{I}^{ref}$ with discharge variability k is shown in Figure 2 for various values of γ. For $\gamma < 1$, $\bar{I}^{ref}$ systematically decreases with increasing discharge variability (i.e., decreasing k). We observe the opposite for $\gamma > 1$. These two regimes have also been found

by *Tucker and Bras* [2000]. For $\gamma = 1$, discharge variability does not affect incision rates. The differences in sensitivity highlight the importance of the incision law exponent a and the local channel geometry (i.e., ω_s), due to their control on the local discharge exponent γ.

[17] For very long return times of Q_m^* (>1000 years), the second term in each of the square brackets in equation (17) becomes negligible. Combining equation (18) and equation (17) then gives an expression of the long-term mean incision rate $\bar{I}$:

$$\bar{I} = \underbrace{\Gamma\left(k/Q_c^*, k+1-\gamma\right)}_{\in[0,1]} \bar{I}^{ref} - \underbrace{\Gamma\left(k/Q_c^*, k+1\right)}_{\in[0,1]} \psi_c. \qquad (19)$$

Equation (19) shows that an erosion threshold reduces the long-term incision rate because (1) not all discharge events cause erosion and (2) each erosive action is diminished by the erosion threshold. Of these two effects, the first is the most important. It is illustrated in Figure 3. It can be seen that reducing the range of erosive events (i.e., increasing Q_c^*) can cancel (case $\gamma = 0.5$ and $Q_c^* = 0.1$ in Figure 3) or reverse the dependency of incision rate on discharge variability for $\gamma \leq 1$ (all cases in Figure 3). As Q_c^* and γ increase, $\bar{I}$ becomes progressively more dependent on discharge variability, a result consistent with findings by *Tucker and Bras* [2000].

[18] Equation (17) is the exact solution of equation (16) for any value of Q_c^* and Q_m^*, but it is not easy to handle
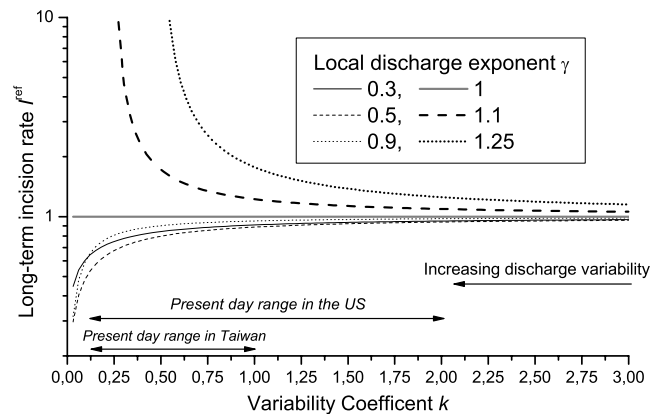
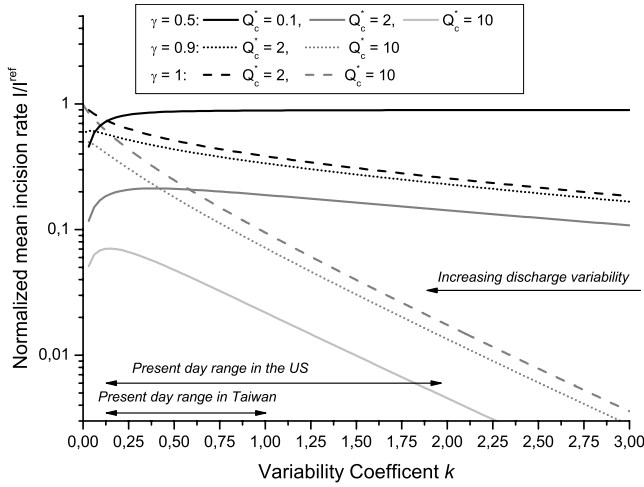**Figure 2.** Variation of long-term incision rate with variability coefficient k for different values of γ.

Figure 3. Mean incision rate in the case of nonnegligible threshold (equation (19)) and very large $\bar{Q}_m^*$, normalized by mean incision rate without threshold $\bar{I}^{ref}$. Figure 3 shows that if the range of erosive events is reduced, the decrease of long-term incision rate with discharge variability observed for negligible threshold (Figure 2) is progressively reversed. For any $\gamma < 1$, there is a particular range of Q_c^* for which the incision rate is almost independent on discharge variability, except for very high variability (for instance, $\gamma = 0.5$ and $Q_c^* = 0.1$).

analytically due to the incomplete gamma functions. Moreover, it is only valid for $\gamma < k + 1$. This is the case for any incision law exponent $a \leq 3/2$, but could not be verified for all values of k for $a > 3/2$ (see Table 1). A simpler approximation can be obtained for cases where the erosive impact of low-flow events (corresponding to the exponential tail of the discharge frequency-magnitude distribution, Figure 1) is negligible. This is true when Q_c^* is large, or when the long-term incision rate is dominated by the largest events ($\gamma \geq k + 1$, for all Q_c^*). Then the frequency-magnitude distribution of erosive discharges (equation (3)) collapses to a power law distribution:

$$pdf_{\bar{Q},k}(Q^*) \simeq \frac{k^{k+1}}{\Gamma(k+1)} Q^{*-(2+k)} dQ^*. \quad (20)$$

Introducing equation (20) in equation (16) gives the following expressions for the long-term incision rate:

$$\bar{I} \simeq \frac{k^{k+1}}{\Gamma(k+1)} \left[\frac{K\bar{Q}^m S^n}{(\gamma - k - 1)} \left(Q_m^{*(\gamma-k-1)} - Q_c^{*(\gamma-k-1)} \right) \right.$$
$$\left. + \frac{\psi_c}{k+1} \left(Q_m^{*-(k+1)} - Q_c^{*-(k+1)} \right) \right], \quad \text{for } \gamma \neq k+1. \quad (21)$$

$$\bar{I} \simeq \frac{(\gamma-1)^\gamma}{\Gamma(\gamma)} \left[K\bar{Q}^m S^n (\ln Q_m^* - \ln Q_c^*) + \frac{\psi_c}{\gamma} (Q_m^{*-\gamma} - Q_c^{*-\gamma}) \right],$$
$$\text{for } \gamma = k+1$$
$$(22)$$

Equations (21) and (22) show that convergence of the incision rate on a constant value with increasing $\bar{Q}_m^*$

depends on the sign of $\gamma - k + 1$. If $\gamma < k + 1$, then any dependency with $\bar{Q}_m^*$ in equation (21) rapidly vanishes with increasing time, and $\bar{I}$ converges on a constant whose approximate expression is:

$$\bar{I} \simeq \frac{k^{k+1}}{\Gamma(k+1)} \left[\frac{K\bar{Q}^m S^n}{(k+1-\gamma)} Q_c^{*-(k+1-\gamma)} - \frac{\psi_c}{k+1} Q_c^{*-(k+1)} \right], \quad (23)$$
$$\text{for } \gamma < k+1.$$

Figure 4 shows that if $k = 0.1$ and $Q_c^* = 1$, then equation (23) is a correct approximation at timescales longer than 100 yr for $\gamma = 0.5$, and 1000 yr for $\gamma = 0.9$. From Figure 4 it is also clear that incision measured over 5 to 10 years permits reasonable approximation of the longer term incision rate (provided that climate and tectonics are stationary). As values of γ between 0.45 and 0.6 are typical of the shear stress model, the incision model favored by us for the purpose of this treatment (see section 4), our results highlight the utility of in situ surveys of bedrock river incision [*Hartshorn et al.*, 2002].

[19] If $\gamma \geq k + 1$, then for increasing $\bar{Q}_m^*$, the terms in Q_c^* become negligible in equations (21) and (22), as is the term with exponent $-(k + 1)$, and we obtain the following expressions:

$$\bar{I} \simeq \frac{k^{k+1}}{\Gamma(k+1)} \frac{K\bar{Q}^m S^n}{(\gamma - k - 1)} Q_m^{*(\gamma-k-1)}, \quad \text{for } \gamma > k+1, \quad (24)$$

$$\bar{I} \simeq \frac{(\gamma-1)^\gamma}{\Gamma(\gamma)} K\bar{Q}^m S^n \ln Q_m^*, \quad \text{for } \gamma = k+1. \quad (25)$$
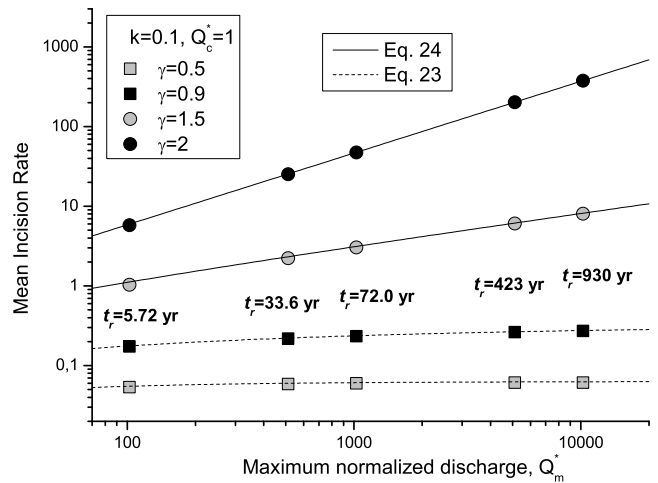

Figure 4. Evolution of mean incision rate with maximum recorded discharge $\bar{Q}_m^*$ for various local discharge exponent γ. Circles are obtained by numerically integrating equation (17). The return time t_r of Q_m^* gives an order of magnitude of the timescale over which incision rate is measured. When $\gamma < k + 1$, the incision rate converges toward a constant value as Q_m^* increases. When $\gamma > k + 1$, the long-term mean incision rate increases approximately as a power function of Q_m^* (equation (24)) with an exponent $\gamma - k - 1$. See color version of this figure in the HTML.
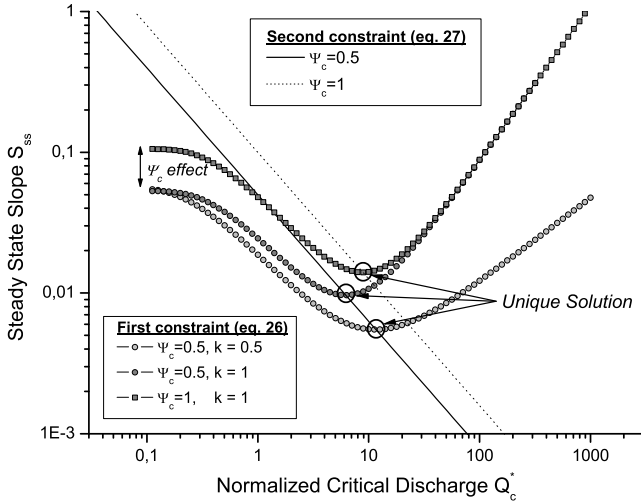
Figure 5. Graphical solution for steady state slope S_{ss} and normalized critical discharge Q_c^*. The first constraint given by equation (26) shows pairs of S_{ss} and Q_c^* of identical long-term incision rate. The second constraint is given by equation (27) and represents values of S_{ss} for which the instantaneous incision rate is zero for $Q^* = Q_c^*$. These two constraints give a unique solution for S_{ss} and Q_c^*. With these parameters ($\gamma = 0.9$, $m = 0.5$, $n = 1$, $K = 1$), S_{ss} and Q_c^* increase with the threshold ψ_c (for constant k). For larger discharge variability (and constant ψ_c), S_{ss} decreases and Q_c^* increases. See color version of this figure in the HTML.

Equations (24) and (25) show that the mean incision rate increases as a power law with the maximum discharge (Figure 4). For any climate, there is a meteorological limit to this predicted increase, and averaged over timescales much longer than the return time of the maximum flood, the mean incision rate reaches a steady value (provided that channel geometry and discharge distribution are steady). For shorter timescales the mean incision rate increases with time (Figure 4). As a consequence, short-term measurements of bedrock incision are likely to be lower than the true long-term incision rate.

3. Climatic and Tectonic Controls on Steady State Slope-Area Relationship

[20] In the previous section we have derived new formulations of a long-term incision law that takes into account the stochasticity of discharge. We have shown that γ controls the sensitivity of incision to discharge variability, and that, depending on its value, the long-term incision rate is governed by Q_c^* (convergent case), or Q_m^* (nonconvergent case). In the following we use this model to explore the longitudinal geometry of bedrock channels, focusing on the long-term steady state in which the discharge regime and the channel geometry remain unchanged for long periods of time. For this condition, the long-term incision rate is constant in time and equal to the rock uplift rate. Whether steady state conditions are likely in natural systems is difficult to assess [*Whipple*, 2001], but in theory the controls (internal and external) on channel geometry can best be identified at steady state. In this study, we consider the convergent case ($\gamma \leq k + 1$) and discuss the nonconvergent

case ($\gamma \geq k + 1$) only briefly, as steady state conditions cannot be attained in this regime (i.e., incision rate can be steady, but the slope has to decrease with time to compensate for the increase of Q_m^*).

3.1. Steady State Slope and Critical Discharge Solution for the Convergent Case

[21] Previous studies have used a simple stream power law model to predict the steady state slope S_{ss} of bedrock channels [*Whipple and Tucker*, 1999]. In addition to this, our model also requires the steady state critical discharge Q_c^* (which is a free parameter in our problem). For this we need two equations (for two unknowns). The first constraint comes from the long-term steady state condition. Assuming a very large maximum discharge Q_m^*, and reformulating equation (17), gives

$$S_{ss}^n = \frac{1}{K} \frac{\Gamma(k+1)k^{-\gamma}}{\Gamma(k+1-\gamma)} \Gamma\left(\frac{k}{Q_c^*}, k+1-\gamma\right)^{-1}$$
$$\cdot \left[\bar{I} + \Gamma\left(\frac{k}{Q_c^*}, k+1\right)\psi_c\right]\bar{Q}^{-m}, \qquad (26)$$

where $\bar{I}$ is the steady state incision rate. The dependency of S_{ss} on Q_c^* predicted by equation (26) is characterized by a unique minimum solution (Figure 5). Below this minimum, when Q_c^* decreases, the slope increases to be just at the threshold condition for $Q^* = Q_c^*$. This effect increases with ψ_c (Figure 5). Above the minimum, S_{ss} increases with Q_c^* to compensate for the reduced range of erosive events, at a rate that depends on k.

[22] A second relationship between S_{ss} and Q_c^* derives from the requirement that the instantaneous incision rate for S_{ss} is zero when $Q^* = Q_c^*$. Using equation (13) this condition is expressed as

$$S_{ss}^n = \left(\frac{\psi_c}{K}\right)\bar{Q}^{-m}Q_c^{*-\gamma}. \qquad (27)$$

[23] There are no analytical solutions for Q_c^* and S_{ss} derived from equations (26) and (27), but a graphical analysis shows a unique intercept of these equations (Figure 5) that seems to coincide with the minimum of equation (26). Deriving equation (26) for Q_c^* and equating it to zero gives the following constraint on Q_c^*

$$Q_c^{*\gamma} = k^{\gamma} \; \psi_c \; \frac{\Gamma(k+1-\gamma)}{\Gamma(k+1)} \frac{\Gamma\left(\frac{k}{Q_c^*}, k+1-\gamma\right)}{\bar{I} + \psi_c\Gamma\left(\frac{k}{Q_c^*}, k+1\right)}, \qquad (28)$$

which can also be found by equating the second terms of equations (26) and (27). This shows that the steady state slope solution is always the unique minimum of equation (26). Hence a river incising at a steady rate is characterized by a unique steady state slope, and a unique normalized critical discharge. This provides a basis for an exploration of the dependency of steady state channel slope and critical discharge on drainage area, incision rate, discharge distribution and incision law parameters. Two approaches are taken: (1) numerical solutions for the general case calculated as the minimum of equation (26) (Figure 5) and (2) approximation using equation (23) when possible to obtain analytical solutions.

3.2. Scaling of Channel Slope With Drainage Area

[24] The relationship between local channel slope and upstream drainage area has been measured in various tectonoclimatic settings [*Hack*, 1957; *Kirby and Whipple*, 2001; *Lague and Davy*, 2003; *Montgomery and Foufoula-Georgiou*, 1993; *Seidl and Dietrich*, 1992; *Sklar and Dietrich*, 1998; *Snyder et al.*, 2000]. It can be modeled by a power law relationship:

$$S = k_s A^{-\theta}, \tag{29}$$

where A is the drainage area. The amplitude factor k_s is often called the steepness index (or channel steepness), and θ is called the channel concavity index (or slope-area exponent). The slope-area relationship has become a fundamental measure of the channel longitudinal geometry. It has been used to calibrate incision laws [*Lague et al.*, 2003; *Lague and Davy*, 2003; *Seidl and Dietrich*, 1992; *Snyder et al.*, 2000, 2003b], estimate uplift rates [*Kirby and Whipple*, 2001; *Lague et al.*, 2000], and validate numerical simulations and theoretical models [*Tucker and Whipple*, 2002; *Willgoose*, 1994]. In particular, prediction of equation (29) is a necessary condition for any incision model.

[25] While the slope-area exponent always falls within a relatively narrow range of values (between 0.4 and 0.6 with some rare measurements down to 0.3 and up to 1; see *Tucker and Whipple* [2002] for a review), the steepness index k_s is known to vary systematically with uplift rate [*Lague et al.*, 2000, 2003; *Snyder et al.*, 2000] and lithology [*Lague et al.*, 2000]. It controls the total channel relief and, to a large extent, the overall relief of fluvially dominated mountain belts [*Lague et al.*, 2003; *Whipple et al.*, 1999]. Understanding and predicting the dependency of k_s with the discharge regime (mean and variability) at steady state thus provides vital information on the link between climate and mountain relief. To our knowledge, this dependency has never received systematic, empirical or theoretical attention. Nevertheless, it is generally believed that most fluvial incision occurs during infrequent large floods [*Baker and Kale*, 1998], and the consensus is that a more variable discharge regime has a greater erosion efficiency. If this were true, then, the steepness of the steady state channel bed ought to be inversely proportional to discharge variability, giving steeper channels for less variable discharge, with incision rate, mean discharge, and all other parameters being equal. In the following, we explore the scaling of channel bed slope and discharge in the context of our incision model.

[26] First, we assume that the daily runoff rate is spatially uniform. This gives the following relationship:

$$Q = RA, \tag{30}$$

where R is the runoff rate. More specifically, the mean runoff rate $\bar{R}$ is defined as the ratio of mean discharge and drainage area. It is assumed to be spatially uniform, as are the discharge variability parameter k and all erosion parameters in equation (13). More complex relationships between discharge variability, runoff and drainage area may occur, and would affect the dependency of channel bed slope and drainage area, but we do not consider such cases

here. Equation (28) shows that the normalized critical discharge Q_c^* is independent of K, m, and n. If $\bar{I}$, ψ_c, γ, k and $\bar{R}$ are spatially uniform, then Q_c^* is independent of drainage area. This being the case, and using equation (27) and equation (30), we obtain the following expression for the slope-area relationship:

$$S_{ss} \propto A^{-\frac{m}{n}}. \tag{31}$$

[27] Our stochastic incision model with threshold predicts a power law relationship between channel bed slope and drainage area that is consistent with observations (equation (29)). The predicted slope-area exponent is the same than for effective discharge models (see, e.g., *Whipple and Tucker* [1999] for $\psi_c = 0$ and *Lague and Davy* [2003] for $\psi_c > 0$) and depends mainly on the scaling of channel width with mean discharge. Note that any systematic spatial variation of incision rate [*Kirby and Whipple*, 2001; *Snyder et al.*, 2003b], mean runoff or runoff variability (related to orographic effects or basin hydrology) [*Roe et al.*, 2002] or any parameter of the incision law (such as the critical shear stress related to downstream changes in the sediment load and caliber) could cause a difference between the measured slope-area exponent in equation (29) and the theoretical prediction of equation (31).

3.3. Runoff Control on Channel Steepness

[28] While the slope-area exponent is independent of discharge conditions (mean and variability) and incision rate, the steepness index depends on these factors in a complex and, in the case of discharge variability, analytically intractable way (equations (26) and (27)). To circumvent this problem, we use numerical solutions to study the impact of discharge variability on channel steepness. In addition, we derive approximate solutions for asymptotic conditions when Q_c^* is either very large or negligible, and the maximum discharge Q_m^* is very large (as is expected for long-term steady state conditions). We assess the conditions for which these expressions are valid, and finally we explore the influence of incision law parameters on channel steepness in the context of a stochastic discharge model.

3.3.1. Impact of Runoff Variability and Mean Runoff on Channel Steepness

[29] We have used numerical solutions to study the impact of runoff variability on channel steepness in the convergent case. Results for the shear stress ($a = 1$) and unit stream power ($a = 3/2$) incision models are presented in Figure 6. Three tendencies can be observed depending on the value of the return time of Q_c^*. When $t_r(Q_c^*) = 1$ day, channel steepness decreases with decreasing discharge variability, as does the erosion efficiency. The opposite is observed when $t_r(Q_c^*) \gg 7$ days. Then, the steepness index increases with increasing discharge variability, and the rate of increase is faster for longer return times of Q_c^*. Between these two regimes where $t_r(Q_c^*)$ is of the order of a week, the steepness index depends only weakly on runoff variability. In this particular case the decrease of erosion efficiency with increasing discharge variability, as found for short return time of Q_c^*, is almost perfectly compensated by the increase of erosion efficiency due to the reduced range of erosive events.
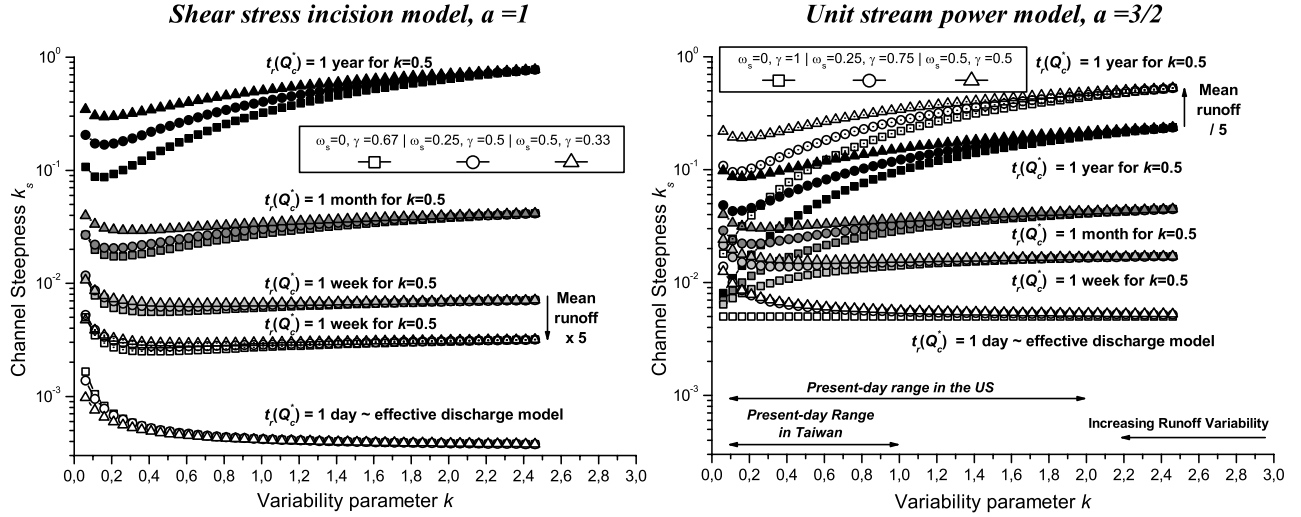
Figure 6. Variations of channel steepness with runoff variability for (left) $a = 1$ and (right) $a = 3/2$. Results are presented for different return times of the critical discharge $t_r(Q_c^*)$ (obtained by increasing the threshold parameter ψ_c with a constant incision rate). Note that the value of $t_r(Q_c^*)$ varies with k (see equation (33)), and the value for k = 0.5 is given for reference. Curves with different exponent γ are normalized by the steepness value at $k = 2.5$ for comparison. The general tendency is toward greater dependency with discharge variability when $t_r(Q_c^*)$ increases. A rectangular channel cross section ($\omega_s = 0$) induces the largest dependency of steepness with variability compared to more concave shapes ($\omega_s > 0$). Fivefold increase or decrease of mean runoff does not affect the variation of steepness with discharge variability. See color version of this figure in the HTML.

[30] Figure 6 also shows that increasing the local discharge-width exponent ω_s (i.e., increasing the concavity of the channel cross section) decreases the sensitivity of the steepness index to discharge variability. For example, the steepness index is predicted to vary by a maximum of 57% for $\omega_s = 0$ and $a = 1$ (84% for $\omega_s = 0$ and $a = 3/2$), and 38% for $\omega_s = 0.5$ and $a = 1$ (32% for $\omega_s = 0$ and $a = 3/2$). The only exception is for the case of the unit stream power model with $t_r(Q_c^*) = 1$ day, where the steepness index is constant for a rectangular channel cross section ($\omega_s = 0$), and increases with discharge variability if $\omega_s > 0$. These results highlight the importance of the local hydraulic geometry which controls the relationship between discharge variability and shear stress variability at the base of the channel.

[31] Because Q_c^* is independent of mean runoff, equation (26) predicts that the steepness index decreases with mean runoff according to:

$$k_s \propto \bar{R}^{-\theta}, \tag{32}$$

where θ is the slope-area exponent. For the same reason, mean runoff does not affect the dependency of k_s with discharge variability (this is also the case for the downstream discharge exponent m, and the erodibility coefficient K). Figure 6 shows that while the magnitude of the steepness index responds to changes in mean runoff according to equation (32), the variation of the steepness index with runoff variability remains unaffected by such changes.

[32] Theoretical predictions (Table 1) [*Whipple and Tucker*, 1999] and surveys of bedrock channels [*Tucker and Whipple*, 2002] give values of θ around 0.5. Hence to first order the effect of mean runoff on channel geometry outweighs the impact of runoff variability for almost all cases where $k > 1$, or return times of the critical discharge

are less than about a month (Figure 6). Only when $t_r(Q_c^*) >$ 1 month and k < 1, both mean runoff and runoff variability affect the steepness of channel. Thus $t_r(Q_c^*)$ at steady state largely determines the control of runoff variability on channel steepness. Accordingly, we have derived an approximation of $t_r(Q_c^*)$ for large Q_c^* (Appendix A):

$$t_r(Q_c^*) \simeq \frac{\gamma}{1 + k - \gamma} \frac{\psi_c}{\bar{I}}. \tag{33}$$

Testing various combinations of parameters, we have found equation (33) to be a good approximation of equation (6) at steady state for $t_r(Q_c^*) \geq 7$ days (Figure 7).

[33] Equation (33) illustrates the relative importance of incision rate, incision law parameters (k_e, τ_c and a through ψ_c) and the local discharge exponent in setting the sensitivity of channel steepness to discharge variability. Specifically, $t_r(Q_c^*)$ is proportional to the ratio of the incision threshold parameter over incision rate. Hence factors increasing the sensitivity of channel steepness to runoff variability at steady state (for $t_r(Q_c^*) \geq 7$ days) are low incision rates, large critical shear stress, weak rocks, and nonlinearity of the shear stress incision law (through the dependency of ψ_c and γ with the incision exponent a). We note that channel steepness is expected to be more sensitive to runoff variability in rivers incising weak rocks, than in rivers incising strong rocks, for the same critical shear stress and incision rate. This is because the steady state slope is comparatively larger for stronger, less erodible rocks, causing the critical shear stress to be overcome more often than in less steep channels in weaker rocks. Equation (33) also illustrates the impact of the cross-sectional channel geom-
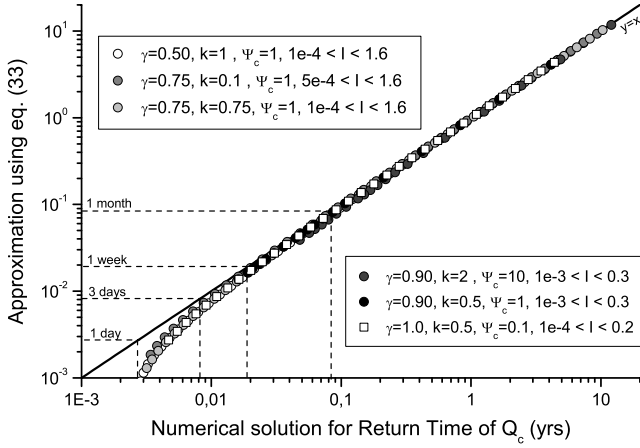
Figure 7. Comparison of numerical solution for the return time of the critical discharge Q_c^* (calculated from the minima of equation (26)) and the approximation given by equation (33). See color version of this figure in the HTML.

etry on the sensitivity of channel steepness to discharge variability (Figure 6). A rectangular channel cross section maximizes γ and increases $t_r(Q_c^*)$ compared to a concave cross section. Consequently, rectangular channels are more sensitive to runoff variability than concave ones (Figure 6).

3.3.2. Scaling of Channel Steepness With Incision Rate and Discharge Variability

[34] Next, we look for asymptotic solutions of k_s for $t_r(Q_c^*) \sim 1$ day, and for very large $t_r(Q_c^*)$, in order to determine the expected relationship between channel steepness, steady state incision rate, and discharge variability. This relationship is of fundamental importance, because it determines the topographic signature of spatially varying incision rates, and its sensitivity to runoff variability. It has been defined for nonstochastic models with threshold [*Lague et al.*, 2003; *Snyder et al.*, 2003a], and explored numerically in a stochastic discharge context by *Tucker* [2004]. However, we are not aware of an analytical solution for a realistic stochastic discharge model.

[35] When Q_c^* is negligible ($t_r(Q_c^*) \sim 1$ day, i.e., the equivalent of an effective discharge model), the incomplete gamma functions in equation (26) are equal to unity, and equation (26) gives the following expression for k_s:

$$k_s = K^{-\frac{1}{n}} \bar{R}^{-\frac{m}{n}} \cdot \left(\frac{\Gamma(k+1)k^{-\gamma}}{\Gamma(k+1-\gamma)} \right)^{\frac{1}{n}} (\psi_c + \bar{I})^{\frac{1}{n}}. \quad (34)$$

In contrast, when Q_c^* is very large the assumption of a power law frequency-magnitude distribution discharge holds, and this allows the use equation (23) as an approximation of the incision rate. By introducing the expression of Q_c^* derived from equation (27) we obtain the following expression for k_s:

$$k_s \simeq K^{-\frac{1}{n}} \bar{R}^{-\frac{m}{n}} \cdot \left(\frac{(k+1)(k+1-\gamma)\Gamma(k+1)}{k^{k+1}\gamma} \right)^{\frac{\gamma}{n(k+1)}} \psi_c^{\frac{k+1-\gamma}{n(k+1)}} \bar{I}^{\frac{\gamma}{n(k+1)}}. \quad (35)$$

This is only valid for $t_r(Q_c^*) \gg 1$ days and $\gamma < k + 1$. Figure 8 shows the quality of the two approximations as a function of

$t_r(Q_c^*)$. Equation (34) is satisfactory for critical discharge return times of up to 1.5 days. Equation (35) is always satisfactory for return times greater than 100 days, and down to 10 days or less for very variable discharges (small k) and/or small local discharge exponent γ.

[36] Equations (34) and (35) show that there is a significant difference in the relation between channel steepness, discharge variability and incision rate between cases with large $t_r(Q_c^*)$ and cases with negligible $t_r(Q_c^*)$. Equation (34) is similar to the prediction obtained by others [*Lague et al.*, 2003; *Snyder et al.*, 2003a] using a constant discharge model with threshold, but it includes explicitly both runoff variability and mean runoff. It predicts that for very large incision rates, the steepness index should scale approximately with incision rate to the power $1/n$ (and exactly if the critical shear stress is zero [*Lague et al.*, 2003; *Snyder et al.*, 2000]). This can be compared with the prediction from equation (35) for the case of relatively large $t_r(Q_c^*)$:

$$k_s \propto \bar{I}^\phi, \quad (36)$$

where the steepness-incision exponent ϕ is

$$\phi = \frac{\gamma}{(1+k)} \frac{1}{n}, \quad \text{for } t_r(Q_c^*) \gg 1 \text{ days}. \quad (37)$$

Figure 9 summarizes some numerical solutions of equations (26) and (27) for steepness index versus incision rate relationships that show the transition between asymptotic regimes for various discharge variabilities. Because the return time of Q_c^* is roughly inversely proportional to incision rate (equation (33)), the power law behavior in equation (35) is fully developed at low incision rates (relative to the threshold parameter). Figure 9 illustrates the three regimes observed in Figure 6. At low incision rates relative to the threshold parameter, k_s decreases with runoff variability, but it increases with decreasing runoff variability at high incision rates when the threshold parameter is negligible. Between these two regimes, there is a small
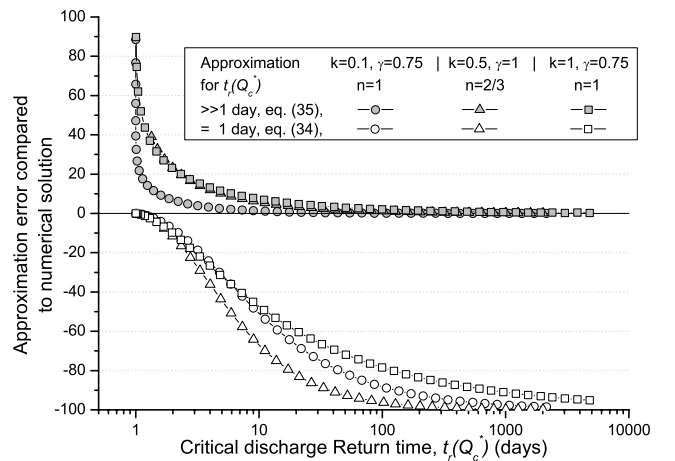

Figure 8. Comparison of the quality of the asymptotic approximation of the steepness index using equations (34) (constant discharge model) and (35) (asymptotic discharge model for large Q_c^*) as a function of the return time of Q_c^* for various incision and discharge condition parameters.
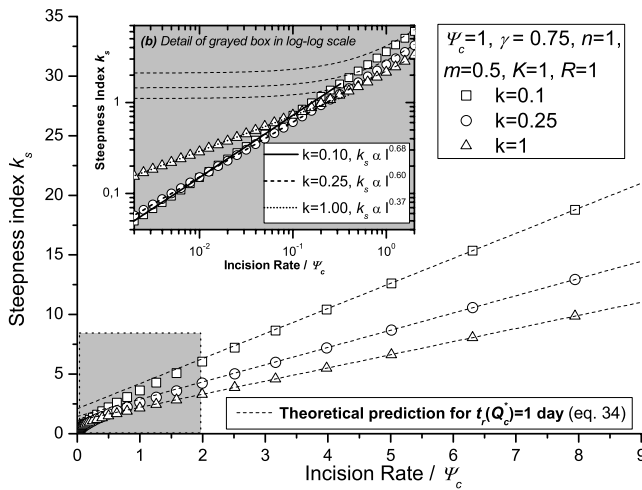
Figure 9. Numerical solutions for the relationship between channel steepness and steady state incision rate for three discharge variability coefficient k. Insert is a log-log plot of the same data focusing on small incision rates and highlighting the power law relationship predicted by equation (35). Units are arbitrary. For low incision rates the steepness-uplift power law exponent ϕ increases with the runoff variability (see equation (37)). For large incision rate (compared to the threshold parameter ψ_c) the relationship corresponds to the predictions of a constant effective discharge model ($t_r(Q_c^*) = 1$ day). In this regime (and for $\gamma \leq 1$) the steady state steepness increases with runoff variability for a given incision rate. This is the opposite for low incision rates. See color version of this figure in the HTML.

range of incision rates (roughly 0.1 to 0.2 times the threshold parameter) for which channel steepness is only weakly dependent on discharge variability.

[37] *Snyder et al.* [2003b] and *Tucker* [2004] have first recognized the deviation from ''constant discharge'' scaling of steepness index with uplift rate, when a significant proportion of runoff events are not erosive. Our results show that this deviation takes the form of a power law relationship between steepness and uplift rate (equation (35) and Figure 9). Equation (37) shows that the channel steepness-incision exponent ϕ is strongly dependent on discharge variability and systematically smaller than the asymptotic value for constant discharge models (as $\gamma < k + 1$ in the present case). An important consequence is that the steady state steepness of channels with variable discharge becomes increasingly dependent on incision rate with increasing runoff variability (Figure 9).

3.4. Nonconvergent Case

[38] Assuming that the maximum value of a is 5/2 [*Whipple et al.*, 2000], and that the channel cross section is slightly concave ($\omega_s = 0.25$), the nonconvergent regime should only occur for the rare case of $k < 0.13 - 0.25$ (see Table 1). Nevertheless, we pursue this case for the sake of completeness. In this regime, the long-term incision rate is heavily dependent on the maximum discharge Q_m^* (equations (24) and (25)) and increases with time for steady state discharge conditions (Figure 4). This precludes a steady state incision rate, unless channel slope decreases with time

to compensate for the increased probability of very large discharges, which in turn precludes topographic steady state. Thus we cannot predict the steady state slope-area relationship in this regime. However, because of their dependency on Q_m^*, the incision rate and the channel steepness are very sensitive to changes in discharge variability. Specifically, we expect an increase in discharge variability to increase incision rates, and decrease channel steepness. These conditions are similar to those studied by *Molnar* [2001] for bed load transport, in which mean runoff has a minimal control on incision rates compared to runoff variability.

4. Discussion

[39] We have used a stochastic approach to upscale bedrock incision from daily to geological timescales in order to study the impact of runoff variability on bedrock river incision and steady state channel steepness. In the following, we discuss similarities and differences of our results with the work of *Snyder et al.* [2003b], *Tucker* [2004], and *Tucker and Bras* [2000], review the limitations of our approach, and seek to improve constraints on the effect of runoff variability on incision in natural systems. Finally, we consider the scaling between channel steepness and incision rate, and the response of bedrock channels to change in mean runoff and runoff variability, and its impact on the coupling of climate and crustal deformation.

4.1. Comparison With Previous Work

[40] Although we have used a different discharge magnitude-frequency distribution, most of our results are qualitatively consistent with the findings of *Tucker and Bras* [2000] and *Tucker* [2004]. We confirm that the efficiency of channel incision can increase with runoff variability if the incision threshold is high compared to the incision rate (a $\leq$ 3/2), and/or if the incision law is very nonlinear with respect to shear stress ($a > 3/2$) [*Tucker and Bras*, 2000]. We also predict the same slope-area exponent and demonstrate that the combination of a nonnegligible threshold of erosion and a stochastic discharge distribution significantly alters the relationship between channel steepness and incision rate predicted by effective discharge models [*Snyder et al.*, 2003b; *Tucker*, 2004]. However, we use a frequency-magnitude distribution of discharge characterized by a ''heavy'' tail, with power law scaling of the pdf of floods, as opposed to an ''exponential'' tail (Figure 1), making it possible to explore regimes in which the extreme floods have a greater importance than in a Poisson model. Use of discharge distributions with an exponential tail would not lead to prediction of a nonconvergent case when $\gamma > k + 1$. An additional, unexpected outcome of the use of discharge distributions with a power law tail is that analytical solutions for the long-term incision rate and the slope-area relationship are easier to obtain (provided that $t_r(Q_c^*) \geq$ 7 days). To our knowledge, such solutions cannot be obtained with a Poisson model for runoff, and demand a numerical treatment instead (G. Tucker, personal communication, 2005). Finally, we demonstrate that the relationship between channel steepness and incision rate is always a power law for large enough $t_r(Q_c^*)$. This is also the case for the Poisson model with large threshold [*Snyder et al.*, 2003b]. However, we demonstrate that the power law exponent is independent

of the incision law exponent a, and depends only on runoff variability and the at-a-station hydraulic geometry of the channel (see equation (38)). It remains to be seen if such result is predicted with a Poisson model.

4.2. Limits to the Approach

[41] We have simplified aspects of the climate-incision system at two different levels: the discharge distribution model and the hydraulic geometry of the channel. Inherent in our stochastic modeling approach is the assumption that runoff events are uncorrelated, or more precisely, that temporal correlations (such as seasonality of flow) do not change the long-term incision rate. This is true as long as the erosion parameters (k_e, τ_c and a) are independent of the runoff history. It could be argued that the assumption does not hold when sediment supply is a significant control on incision rate. For example, a large flood could result in the alluviation of the channel and stop incision until the sediment cover has been removed by subsequent discharge events. However, we postulate that these mantling events are likely to be short-lived compared to the geological timescale of our study [Benda and Dunne, 1997a, 1997b]. Temporary mantling may contribute significantly to high-frequency variations of incision rates [Pratt et al., 2004], but its effects are probably smoothed out over longer timescales (provided that climate is steady). The discharge frequency-magnitude distribution model we have used is one of the most complete, but further work is required to quantify the range of possible values for the variability parameter k and to assess its applicability to various climate settings.

[42] Our analysis has underlined the importance of the hydraulic geometry of bedrock channels: the downstream variation of channel width is a first-order control on the scaling of steady state channel steepness with mean runoff, and the local variation of flow width with discharge controls the scaling of channel steepness with runoff variability and incision rate. The variation of the local flow width with discharge has a previously unsuspected importance due to its strong influence on the scaling of mean basal shear stress and daily discharge. Our analysis relies on an under-constrained empirical expression for the local (i.e., at-a-station) hydraulic geometry (equation (11)), but it is sufficiently general to encompass cases where channel width is constant (vertical walls) or variable with discharge (concave up walls). Adopting an alternative expression would obviously affect our analysis, but not change our conclusions. We point out that as mean channel width is specified as a function of discharge (equation (10)), it does change for a given drainage area when the mean runoff is changed. However, the proportionality coefficient k_w might depends on the rock resistance and possibly on the incision rate and/or sediment supply in a way that is not yet understood [Duvall et al., 2004; Lavé and Avouac, 2001]. The same is true for the local discharge exponent which depends on the flow variability (this sets the variation of flow stage and thus controls the vertical extent of lateral erosion and the resulting wall shape and cross-sectional geometry), and potentially on rock resistance, incision rate and sediment supply. Importantly, we have assumed that a steady state cross-sectional geometry is attained. It is likely that this is appropriate for the downstream hydraulic geometry as is indicated by several studies which have reported

power law relationships similar to equation (10) with an exponent $\omega_a \approx 0.5$ [Montgomery and Gran, 2001; Snyder et al., 2003a]. However, this assumption remains to be confirmed for the cross-sectional geometry. We conclude that there is an urgent need for precise documentation of the hydraulic geometry of bedrock channels in the context of forcing parameters to improve our modeling ability.

4.3. Estimates of $t_r(Q_c^*)$ in Mountain Channels

[43] Incision of bedrock channels is not a continuous process. Most of the mechanisms thought to be important in bedrock incision operate only above a discharge threshold. Although dissolution can occur in the full range of flow conditions in bedrock channels, plucking and impact abrasion by saltating bed load require a minimum shear stress to detach blocks of rock or transport bed load that is not achieved in low-flow conditions [Snyder et al., 2003b], and cavitation requires very high discharges [Whipple et al., 2000]. Accordingly, we do not expect that the asymptotic predictions for critical discharge with a return time of 1 day (equation (34)) are likely to apply in natural systems. However, they may be relevant to small-scale laboratory experiments in which runoff has a limited variability. In such experiments, the steepness-incision relationship predicted by equation (34) has in fact been observed [Lague et al., 2003].

[44] There is evidence that in areas with high rock uplift rate (>1 mm yr^{-1}) incision does occur frequently (return times less than a month). The first line of evidence comes from direct in-situ measurement of bedrock incision in a Taiwanese river. In a companion paper (D. Lague et al., Calibration of a bedrock incision model in Li-Wu River, Taiwan, manuscript in preparation, 2005), we use incision measurements across the river channel taken at 6-month intervals (see Hartshorn et al. [2002] for details) and daily measurements of water discharge to estimate Q_c^*. In this area, the long-term exhumation rate is high (3–6 mm yr^{-1}) and the short-term incision rate is approximately the same [Hartshorn et al., 2002]. The frequency-magnitude distribution of discharges at the study site is well described by equation (1), with $k = 0.5$ and $\bar{Q} = 34$ m^3 s^{-1}. We estimate $t_r(Q_c^*)$ to be of the order of 20 days for a bedrock rib protruding 1 m above the lowest point in the channel, with incision occurring mainly during the summer typhoon season period. We have extrapolated this result to the river thalweg, where we do not have measurements of wear, and found that $t_r(Q_c^*) = 7$–10 days. In this river, thalweg lowering occurs ~10–15% of all days.

[45] The second constraint comes from [Snyder et al., 2003b] who have used a calibrated frequency-magnitude distribution of daily rainfall paired with a shear-stress incision law identical to equation (8) to estimate k_e and τ_c from the variation of bedrock channel steepness with uplift rate in the Mendocino Triple Junction area. With these parameters, they have estimated that $t_r(Q_c^*) \sim 5.3$–14.3 days when $\bar{I} \sim 4$ mm yr^{-1}, and $t_r(Q_c^*) \sim 50$–333 days when $\bar{I} \sim 0.5$ mm yr^{-1}. Uncertainties in the estimate of $t_r(Q_c^*)$ are due to the lack of constraint on the exponent a on shear stress in the incision law (equation (7)) that can be either 1 or 3/2 [Snyder et al., 2003b].

[46] These two independent constraints shows that rapid fluvial incision of bedrock could occur very frequently, say

every 6 to 15 days. Consequently, the constant discharge model cannot be used to model bedrock incision (see Figure 8) [*Snyder et al.*, 2003b]. An effective discharge can be defined, but it varies with incision rate, discharge variability and the threshold parameter. This has, so far, not been taken into account in modeling studies. The short return time of the critical discharge does not imply that rare and extreme events do not contribute significantly to long-term incision: their importance relative to more common discharges is set by the value of *a*.

4.4. Calibration of Incision Laws and Estimation of Uplift Rates

[47] At the scale of individual tectonic structures, rivers tend to evolve naturally toward a steady state in which, on longer timescales, incision and rock uplift are equal but opposite. For example, *Lavé and Avouac* [2000] have documented steady state at timescales of 10^4 years in rivers incising sandstones at rates of 5 to 15 mm yr^{-1}. Such settings have received considerable attention because they can be used to validate and calibrate incision laws [*Duvall et al.*, 2004; *Kirby and Whipple*, 2001; *Lague and Davy*, 2003; *Snyder et al.*, 2000, 2003b] that can then be applied to other steady state rivers to estimate local rock uplift rates. Assuming that equation (35) applies (i.e., $t_r(Q_c^*)$ is at least of the order of a week and the incision law exponent *a* is small), we predict that the channel steepness-rock uplift relationship is a power law (equation (36)) whose exponent ϕ is given by equation (37). This can be simplified to

$$\phi = \frac{\alpha(1 - \omega_s)}{\beta(1 + k)}. \tag{38}$$

Contrary to what is predicted by a "constant discharge" model ($\phi = 1/\beta a$) [*Lague and Davy*, 2003; *Snyder et al.*, 2000; *Whipple et al.*, 1999], equation (38) shows that ϕ is independent of the incision law exponent *a*, and depends only on runoff variability and the at-a-station hydraulic geometry of the channel (α and β being approximately equal). Using values of *k* between 0.1 and 2.5 and values of ω_s between 0 and 0.5, we find that ϕ is between 0.15 and 0.9. This is consistent with estimates by *Snyder et al.* [2000] ($\phi = 0.26$) for bedrock channels and by *Lague and Davy* [2003] ($\phi = 0.32$) for colluvial channels, even though the flow resistance equations and hydraulic geometry differ from those in bedrock channels. Note that for very variable discharge conditions and a concave channel cross section, mean runoff is more important than incision rate in controlling channel steepness (see equation (32)).

[48] Importantly, it is not possible to calibrate the exponent of a shear-stress incision law of the type of equation (8) using the relationship between channel steepness and rock uplift rate as by *Duvall et al.* [2004], *Lague and Davy* [2003], and *Snyder et al.* [2000, 2003b]. However casting equation (35) in terms of a long-term incision rate gives

$$\bar{I} = a\alpha(1 - \omega_s)k_e\tau_c^a\tau_c^{-\frac{(k+1)}{\alpha(1-\omega_s)}}\left(\frac{k_t}{k_w^\alpha}\right)^{\frac{k+1}{\alpha(1-\omega_s)}}$$
$$\cdot \left(\frac{k^{k+1}\Gamma(k+1)^{-1}}{(k+1)(k+1-a\alpha(1-\omega_s))}\right)\bar{Q}^{\frac{(1-\omega a)(k+1)}{(1-\omega_s)}}S^{\frac{\beta(k+1)}{\alpha(1-\omega_s)}}. \tag{39}$$

In equation (39) the incision exponent *a* no longer applies to the channel slope, the amplitude factor of the channel width (k_w), and the mean runoff. Although *a*, k_e and τ_c remain underconstrained, it is possible in theory to estimate the spatial variations of the steady state incision rate provided that (1) the spatial distributions of $\bar{Q}$, S, k_t and k_w (or the flow width corresponding to the mean discharge) are known (or only $\bar{Q}$ and S are variable), (2) the other parameters (including the flow variability) are spatially uniform, (3) the steady state holds and (iv) $t_r(Q_c^*)$ is greater than 1 week (i.e., equation (35) is valid). Using a method similar to the one proposed by *Lague et al.* [2000], it should be possible to calculate the spatial distribution of incision rates if the incision rate is known at one location along the river. If a value for *a* is assumed, then spatial variations in runoff variability can be fully taken into account, avoiding the choice of an "effective discharge" [*Lavé and Avouac*, 2001]. If $t_r(Q_c^*)$ and the incision rate are known, ψ_c can also be calibrated using equation (33).

[49] Equation (39) is a generalized version of the stream power law model of bedrock incision in the case of steady state incision. It is the first expression to fully take into account a threshold of erosion and the frequency-magnitude distribution of runoff. The traditional discharge exponent *m* and slope exponent *n* are independent of the incision law, but strongly dependent on the runoff variability and the hydraulic geometry of the channel. Typical values for *m* and *n* in a very variable climate would be around 1 and 2, respectively ($\omega_a = 0.5$, $\omega_s = 0.25$, $k = 0.5$, $\alpha = \beta$), and in an steady climate ($k = 1.5$) around 1.67 and 3.33, respectively. These values are significantly larger than those normally used (Table 1), underlining the nonlinearity introduced by an erosion threshold and a reduced range of erosive events. Equation (39) also provides an alternative explanation for the increase in the erosion efficiency with incision rate observed by various authors [*Duvall et al.*, 2004; *Snyder et al.*, 2000] (i.e., a deviation from theoretical predictions using a constant effective discharge model). This result is expected within the context of a stochastic discharge model with threshold [see also *Snyder et al.*, 2003b; *Tucker*, 2004], but we note that it could also be attributed to a decrease of channel width with incision rate [cf. *Duvall et al.*, 2004].

4.5. Climate and Incision Efficiency of Mountain Channels

[50] Using the shear stress incision model of equation (8), we have shown that the introduction of discharge variability can significantly increase the erosion efficiency of bedrock channels, but only when the incision threshold is very high relative to the incision rate (i.e., $t_r(Q_c^*) > 1$ month, see Figure 6). Discharge variability is also important in the nonconvergent regime, but this covers only a very limited range of extremely variable climates and incision laws, unlikely to apply in many bedrock rivers. While the exact formulation of incision laws such as the one we used is subject to debate, *Lavé and Avouac* [2001] have demonstrated that equation (8) with $a = 1$ and k_e inversely proportional to the grain size transported in the river predicts precisely the pattern of river incision over 10^4 years, along Himalayan rivers incising at rates between 5 and 17 mm yr^{-1}. In Appendix B, we show how the model of bedrock incision by saltating bed load proposed by *Sklar*

and Dietrich [2004] can be rewritten as a simple shear-stress incision model with $a = 1$ and k_e a complex function of grain size, rock mass properties and the ratio of sediment supply to sediment transport capacity.

[51] If $a = 1$ and k_e are independent of runoff conditions, and assuming that $t_r(Q_c^*)$ is about 4 to 15 days in rapidly incising bedrock rivers, we predict that runoff variability has probably no measurable impact on the steady state steepness of bedrock channels. Hence the main "climatic" control on channel steepness and incision efficiency is mean runoff. Its effect on longitudinal channel geometry is given by equation (32). This expression suggests that if climate were to evolve toward drier but more variable conditions, the river incision rate would decrease, and with it the catchment-wide long-term denudation rate in fluvially dominated areas, and channel steepness would increase. Such a climate change has been invoked as a possible explanation for the observed increase in global sedimentation rates during the Late Cenozoic [*Molnar*, 2001; *Zhang et al.*, 2001]. Our analysis is not consistent with this postulate. Whether this is due to misestimation of the return time of the critical discharge required for fluvial bedrock incision, inadequacy of the bedrock incision model or the climate model, or indeed an argument in favor of glacial erosion remains to be determined.

5. Conclusion

[52] We have coupled a realistic stochastic distribution of discharge with a deterministic incision law to predict the influence of mean runoff and runoff variability on long-term incision rates and steady state channel steepness. Our approach improves on earlier attempts by using a frequency-magnitude distribution of discharge that encompasses the entire range of discharges, and, most importantly, reproduces the power law tailing of rare and extreme events. Calculating long-term incision rates by integrating the action of all discharge events weighted by their probability of occurrence, we predict fluvial incision rates to converge rapidly ($\sim 10^2 - 10^3$ years) toward a constant value for all cases except the rare situation in which discharge is extremely variable ($k < 0.1 - 0.25$) and the incision law very nonlinear ($a = 5/2$). Our model predicts a power law scaling between slope and drainage area whose exponent is independent of the runoff conditions (mean and variability), and consistent with observations. The predicted steady state channel steepness decreases approximately as the inverse of the square root of mean runoff. Runoff variability has a more complex effect, characterized by three regimes with different return times of the critical discharge required for fluvial incision: if the return time is ~ 1 day, the channel steepness increases with runoff variability; for return times between 1 day and about 1 month, the channel steepness depends weakly on runoff variability; for longer return times, the channel steepness decreases with runoff variability. We have found that the return time of the critical discharge is about a week in rapidly incising bedrock rivers (≥ 4 mm yr^{-1}), so that their steepness is likely to be controlled by the mean runoff rather than the runoff variability. Because the return time of the critical discharge is proportional to the ratio of the incision threshold term over the uplift rate, runoff variability could be important in

bedrock rivers incising at slow rates (<1 mm yr^{-1}?) and/or into weaker substrates. We have also demonstrated that a stochastic model with incision threshold predicts a power law relationship between channel steepness and incision rate whose exponent is independent of the incision law exponent on shear stress. This highlights a fundamental difference with effective discharge models in which the incision law exponent is thought to controls the scaling of channel steepness with incision rate at steady state. Recognizing this difference, we have presented a new expression for the long-term incision rate at steady state that has the form of a stream power law without threshold, but whose exponent on slope and discharge are independent of the incision law exponent a, and larger than in the case of an effective discharge model.

[53] Possibly our most surprising prediction is that mean runoff, rather than runoff variability and incision rate, could be the dominant control on channel steepness, although this result remains to be tested. Our results highlight the necessity of a stochastic discharge approach to the modeling of bedrock incision, and the importance of the incision threshold as a fundamental parameter of incision laws [*Davy and Crave*, 2000; *Molnar*, 2001; *Snyder et al.*, 2003b; *Tucker*, 2004; *Tucker and Bras*, 2000]. Our analysis also stresses the importance of the local discharge exponent for the scaling of channel steepness with runoff variability and incision rate. It depends largely on the cross-sectional shape of bedrock rivers, an aspect of river geometry that has rarely been documented. In bedrock channels incising cohesive rocks, the cross-sectional shape results from the competition between uplift and abrasion processes by bouncing blocks and suspended particles. On longer timescales, this competition is modulated by the probability of occurrence of high discharge events during which lateral erosion occurs [*Hartshorn et al.*, 2002]. Full documentation of lateral channel dynamics is a critical requirement for progress in the understanding of river erosion and landscape evolution.

Appendix A:　Approximation of $t_r(Q_c^*)$ at Steady State

[54] When the critical discharge is large enough, the frequency-magnitude distribution of erosive discharges can be approximated by a power law according to equation (20). Then according to equations (4) and (20),

$$t_r(Q_c^*) = \left[\int_{Q_c^*}^{+\infty} \frac{k^{k+1}}{\Gamma(k+1)} Q^{*-(2+k)} dQ^* \right]^{-1}. \quad \text{(A1)}$$

Equation (A1) simplifies into

$$t_r(Q_c^*) = \frac{(k+1)\Gamma(k+1)}{k^{k+1}} Q_c^{*(1+k)}. \quad \text{(A2)}$$

Using the expression of Q_c^* derived from equation (27) and the expression of steady state slope derived from equation (35), we obtain the following expression of Q_c^*:

$$Q_c^* = \left(\frac{\gamma k^{k+1}}{(k+1)(k+1-\gamma)\Gamma(k+1)} \frac{\Psi_c}{\bar{I}} \right)^{\frac{1}{k+1}}, \quad \text{(A3)}$$

that gives

$$t_r(Q_c^*) \simeq \frac{\gamma}{1 + k - \gamma} \frac{\psi_c}{\bar{\bar{I}}} \tag{A4}$$

Appendix B: Simplification of the Sklar and Dietrich Model Into a Simple Shear-Stress Model

[55] We use the general expression for bedrock incision by saltating bed load derived from equation (24b) of *Sklar and Dietrich* [2004]:

$$I = \frac{0.08 R_b g Y}{k_v \sigma_t^2} q_s \left(\frac{\tau^*}{\tau_c^*} - 1 \right)^{-0.52} \left(1 - \frac{q_s}{q_t} \right) \tag{B1}$$

where R_b is the nondimensional buoyant density $[(\rho_s - \rho)/\rho]$, Y is Young's modulus of elasticity [Mpa], k_v is a rock resistance coefficient (empirically calibrated), σ_t is the rock tensile strength [Mpa], q_s is the unit sediment supply, q_t is the unit sediment transport capacity, τ^* is the Shield's stress and τ_c^* is the critical Shield's stress. Following *Sklar and Dietrich* [2004], we have neglected the suspension term that is originally in their equation (24b).

[56] The difficulty when upscaling equation (B1) to longer timescales is to define how sediment supply scales with shear stress. We assume that the daily unit sediment supply is a fixed proportion of the daily sediment transport capacity:

$$q_s = \phi q_t, \tag{B2}$$

where ϕ varies between 0 and 1. It means that the daily unit sediment supply rate has the same scaling with shear stress than the sediment transport capacity. This makes sense if the contribution from the local hillslopes is negligible compared to the bed load supply from upstream. Equation (B2) insures that the long-term ratio between sediment supply and sediment transport capacity is ϕ. In the modeling framework of Sklar and Dietrich, it also means that sediment cover is identical for all discharge stages. The unit sediment transport capacity law used by *Sklar and Dietrich* [2004] is

$$q_t = 5.7 \rho_s \left(R_b g D_s^3 \right)^{1/2} (\tau^* - \tau_c^*)^{3/2} = 5.7 \frac{\rho_s}{\rho(\rho_s - \rho)g} (\tau - \tau_c)^{3/2} \tag{B3}$$

and using equation (B2) in equation (B1), we obtain the following expression for the daily incision rate:

$$I = 0.456 \frac{Y}{k_v \sigma_t^2} \frac{\rho_s}{\rho^2} \tau_c^{1/2} (\tau - \tau_c) \phi(1 - \phi). \tag{B4}$$

Equation (B4) is a simple shear stress incision law ($a = 1$).

Notation

Q daily discharge.
$\bar{Q}$ mean daily discharge.
k variability parameter.

Q^* normalized daily discharge.
R daily runoff.
$\bar{R}$ mean daily runoff.
$t_r(Q^*)$ return time of discharge Q^*.
Q_c^* normalized critical discharge for incipient incision.
Q_m^* maximum normalized discharge.
$\bar{I}$ mean long term incision rate.
$\bar{\bar{I}}$ mean long term incision rate without threshold.
I daily incision rate.
k_e incision efficiency coefficient.
τ basal shear stress.
τ_c critical shear stress for incision.
a incision law exponent.
k_t hydraulic friction factor.
W flow width.
S channel slope.
A drainage area.
k_s steepness index.
θ concavity index.
ϕ steepness/incision scaling exponent.
α, β exponents of the flow resistance equation.
ω_s local (at-a-station) scaling exponent between flow width and discharge.
ω_a downstream scaling exponent between channel width and discharge.
w_a flow width corresponding to the mean discharge.
k_w amplitude factor of the channel width/mean discharge relationship.
K erodibility factor.
m downstream discharge exponent.
γ local discharge exponent.
n slope exponent.
ψ_c threshold parameter.

References

Baker, V. R., and V. S. Kale (1998), The role of extreme floods in shaping bedrock channels, in *Rivers Over Rock: Fluvial Processes in Bedrock Channels*, Geophys. Monogr. Ser., vol. 107, edited by K. J. Tinkler and E. E. Wohl, pp. 53–165, AGU, Washington, D. C.

Baldwin, J. A., K. X. Whipple, and G. E. Tucker (2003), Implications of the shear stress river incision model for the timescale of postorogenic decay of topography, *J. Geophys. Res.*, 108(B3), 2158, doi:10.1029/2001JB000550.

Beaumont, C., P. Fullsack, and J. Hamilton (1992), Erosional control of active compressional orogens, in *Thrust Tectonics*, edited by K. R. McClay, pp. 1–18, CRC Press, Boca Raton, Fla.

Benda, L., and T. Dunne (1997a), Stochastic forcing of sediment routing and storage in channel networks, *Water. Resour. Res.*, 33, 2865–2880.

Benda, L., and T. Dunne (1997b), Stochastic forcing of sediment supply to channel networks from landsliding and debris flow, *Water Resour. Res.*, 33, 2849–2863.

Braun, J., and M. Sambridge (1997), Modelling landscape evolution on geological time scales: A new method based on irregular spatial discretization, *Basin Res.*, 9, 27–52.

Clift, P., J. I. Lee, M. K. Clark, and J. Blusztajn (2002), Erosional response of South China to arc rifting and monsoonal strengthening: A record from the South China Sea, *Mar. Geol.*, 184, 207–226.

Crave, A., and P. Davy (2001), A stochastic "precipiton" model for simulating erosion/sedimentation dynamics, *Comput. Geosci.*, 27, 815–827.

Davy, P. (1993), On the frequency-length distribution of the San Andreas fault system, *J. Geophys. Res.*, 98(B7), 12,141–12,151.

Davy, P., and A. Crave (2000), Upscaling local-scale transport processes in large-scale relief dynamics, *Phys. Chem. Earth A*, *25*(6–7), 533–541.

Duvall, A., E. Kirby, and D. W. Burbank (2004), Tectonic and lithologic controls on bedrock channel profiles and processes in coastal California, *J. Geophys. Res.*, *109*, F03002, doi:10.1029/2003JF000086.

Ely, L. L. (1997), Response of extreme floods in the southwestern United States to climatic variations in the late Holocene, *Geomorphology*, *19*, 175–201.

Finlayson, D. P., D. R. Montgomery, and B. Hallet (2002), Spatial coincidence of rapid inferred erosion with young metamorphic massifs in the Himalayas, *Geology*, *30*(3), 219–222.

France-Lanord, C., and L. A. Derry (1997), Organic carbon burial forcing of the carbon cycle from Himalayan erosion, *Nature*, *390*, 65–67.

Hack, J. T. (1957), Studies of longitudinal stream profiles in Virginia and Maryland, *U.S. Geol. Surv. Prof. Pap.*, *294B*, 45–94.

Harris, S. E., and A. C. Mix (2002), Climate and tectonic influences on continental erosion of tropical South America, 0–13 Ma, *Geology*, *30*(5), 447–450.

Hartshorn, K., N. Hovius, W. B. Dade, and R. L. Slingerland (2002), Climate-driven bedrock incision in an active mountain belt, *Science*, *297*, 2036–2038.

Hilley, G. E., and M. R. Strecker (2004), Steady state erosion of critical Coulomb wedges with applications to Taiwan and the Himalaya, *J. Geophys. Res.*, *109*, B01411, doi:10.1029/2002JB002284.

Howard, A. D. (1994), A detachment-limited model of drainage basin evolution, *Water Resour. Res.*, *30*(7), 2261–2285.

Howard, A. D., and G. Kerby (1983), Channel changes in badlands, *Geol. Soc. Am. Bull.*, *94*, 739–752.

Kirby, E., and K. Whipple (2001), Quantifying differential rock-uplift rates via stream profile analysis, *Geology*, *29*(5), 415–418.

Knighton, D. (1998), *Fluvial Form and Processes*, 383 pp., Edward Arnold, London.

Kooi, H., and C. Beaumont (1996), Large-scale geomorphology: Classical concepts reconciled and integrated with contemporary ideas via a surface processes model, *J. Geophys. Res.*, *101*(B2), 3361–3386.

Lague, D., and P. Davy (2003), Constraints on the long-term colluvial erosion law by analyzing slope-area relationships at various tectonic uplift rates in the Siwaliks Hills (Nepal), *J. Geophys. Res.*, *108*(B2), 2129, doi:10.1029/2002JB001893.

Lague, D., P. Davy, and A. Crave (2000), Estimating uplift rate and erodibility from the area-slope relationship: Examples from Brittany (France) and numerical modelling, *Phys. Chem. Earth A*, *25*(6–7), 543–548.

Lague, D., A. Crave, and P. Davy (2003), Laboratory experiments simulating the geomorphic response to tectonic uplift, *J. Geophys. Res.*, *108*(B1), 2008, doi:10.1029/2002JB001785.

Lavé, J., and J. P. Avouac (2000), Active folding of fluvial terraces across the Siwaliks Hills, Himalayas of central Nepal, *J. Geophys. Res.*, *105*(B3), 5735–5770.

Lavé, J., and J. P. Avouac (2001), Fluvial incision and tectonic uplift across the Himalayas of central Nepal, *J. Geophys. Res.*, *106*(B11), 26,561–26,591.

Leopold, L. B., and T. J. Maddock (1953), The hydraulic geometry of stream channels and some physiographic implications, *U.S. Geol. Surv. Prof. Pap.*, *252*, 57 pp.

Meybeck, M., L. Laroche, H. H. Dürr, and J. P. M. Syvitski (2003), Global variability of daily total suspended solids and their fluxes in rivers, *Global Planet. Change*, *39*(1–2), 65–93.

Millot, R., J. Gallairdet, B. Dupré, and C. J. Allègre (2002), The global control of silicate weathering rates and the coupling with physical erosion: New insights from rivers of the Canadian Shield, *Earth Planet. Sci. Lett.*, *196*, 83–98.

Molnar, P. (2001), Climate change, flooding in arid environments, and erosion rates, *Geology*, *29*(12), 1071–1074.

Molnar, P., and P. England (1990), Late Cenozoic uplift of mountain ranges and global climate change: Chicken or egg?, *Nature*, *346*, 29–34.

Montgomery, D. R., and E. Foufoula-Georgiou (1993), Channel network source representation using digital elevation models, *Water Resour. Res.*, *29*, 3925–3934.

Montgomery, D. R., and K. B. Gran (2001), Downstream variations in the width of bedrock channels, *Water Resour. Res.*, *37*, 1841–1846.

Olsson, J., and P. Burlando (2002), Reproduction of temporal scaling by a rectangular pulses rainfall model, *Hydrol. Processes*, *16*, 611–630.

Pratt, B., D. W. Burbank, A. Heimsath, and T. Ojha (2004), Landscape disequilibrium on 1000–10,000 year scales, Marsyandi River, Nepal, central Himalaya, *Geomorphology*, *58*, 223–241.

Raymo, M. E., and W. F. Ruddiman (1992), Tectonic forcing of late Cenozoic climate, *Nature*, *359*, 117–122.

Rinaldo, A., W. E. Dietrich, R. Rigon, G. K. Vogel, and I. Rodriguez-Iturbe (1995), Geomorphological signatures of varying climate, *Nature*, *374*, 632–635.

Roe, G. H., D. R. Montgomery, and B. Hallet (2002), Effects of orographic precipitation variations on the concavity of steady-state river profiles, *Geology*, *30*, 143–146.

Roe, G. H., D. R. Montgomery, and B. Hallet (2003), Orographic precipitation and the relief of mountain ranges, *J. Geophys. Res.*, *108*(B6), 2315, doi:10.1029/2001JB001521.

Ruddiman, W. F., and W. L. Preil (1997), Introduction to the uplift-climate connection, in *Tectonic Uplift and Climate Change*, edited by W. F. Ruddiman, pp. 3–15, Springer, New York.

Seidl, M. A., and W. E. Dietrich (1992), The problem of channel erosion into bedrock, *Catena Suppl.*, *23*, 101–124.

Sklar, L., and W. E. Dietrich (1998), River longitudinal profiles and bedrock incision models: Stream power and the influence of sediment supply, in *Rivers Over Rock: Fluvial Processes in Bedrock Channels*, Geophys. Monogr. Ser., vol. 107, edited by K. J. Tinkler and E. E. Wohl, pp. 237–260, AGU, Washington, D. C.

Sklar, L. S., and W. E. Dietrich (2004), A mechanistic model for river incision into bedrock by saltating bed load, *Water Resour. Res.*, *40*, W06301, doi:10.1029/2003WR002496.

Slack, J. R., A. M. Lumb, and J. M. Landwehr (1993), Hydroclimatic data network (HCDN): A U.S. Geological Survey streamflow data set for the United States for the study of climate variation, 1874–1988, *U.S. Geol. Surv. Water Resour. Invest. Rep.*, *93-4076*.

Snyder, N. P., K. X. Whipple, G. E. Tucker, and D. J. Merritts (2000), Landscape response to tectonic forcing: DEM analysis of stream profiles in the Mendocino triple junction region, northern California, *Geol. Soc. Am. Bull.*, *112*, 1250–1263.

Snyder, N. P., K. X. Whipple, G. E. Tucker, and D. J. Merritts (2003a), Channel response to tectonic forcing: Field analysis of stream morphology and hydrology in the Mendocino triple junction region, northern California, *Geomorphology*, *53*(1–2), 97–127.

Snyder, N. P., K. X. Whipple, G. E. Tucker, and D. J. Merritts (2003b), Importance of a stochastic distribution of floods and erosion thresholds in the bedrock river incision problem, *J. Geophys. Res.*, *108*(B2), 2117, doi:10.1029/2001JB001655.

Sobel, E. R., G. E. Hilley, and M. R. Strecker (2003), Formation of internally drained contractional basins by aridity-limited bedrock incision, *J. Geophys. Res.*, *108*(B7), 2344, doi:10.1029/2002JB001883.

Stock, J. D., and D. R. Montgomery (1999), Geologic constraints on bedrock river incision using the stream power law, *J. Geophys. Res.*, *104*(B3), 4983–4993.

Svensson, C., J. Olsson, and R. Berndtsson (1996), Multifractal properties of daily rainfall in two different climates, *Water Resour. Res.*, *32*, 2463–2472.

Tucker, G. E. (2004), Drainage basin sensitivity to tectonic and climatic forcing: Implications of a stochastic model for the role of entrainment and erosion thresholds, *Earth Surf. Processes Landforms*, *29*(2), 185–205.

Tucker, G. E., and R. L. Bras (2000), A stochastic approach to modeling the role of rainfall variability in drainage basin evolution, *Water Resour. Res.*, *36*, 1953–1964.

Tucker, G. E., and R. L. Slingerland (1994), Erosional dynamics, flexural isostasy, and long-lived escarpments: A numerical modeling study, *J. Geophys. Res.*, *99*(B6), 12,229–12,243.

Tucker, G. E., and R. Slingerland (1997), Drainage basin response to climate change, *Water Resour. Res.*, *33*, 2031–2047.

Tucker, G. E., and K. X. Whipple (2002), Topographic outcomes predicted by stream erosion models: Sensitivity analysis and intermodel comparison, *J. Geophys. Res.*, *107*(B9), 2179, doi:10.1029/2001JB000162.

Turcotte, D. L., and L. Greene (1993), A scale-invariant approach to flood-frequency analysis, *Stochastic Hydrol. Hydraul.*, *7*, 33–40.

Whipple, K. X. (2001), Fluvial landscape response time: How plausible is steady-state denudation?, *Am. J. Sci.*, *301*, 313–325.

Whipple, K. X., and B. Meade (2004), Controls on the strength of coupling among climate, erosion, and deformation in two-sided, frictional orogenic wedges at steady state, *J. Geophys. Res.*, *109*(F1), F01011, doi:10.1029/2003JF000019.

Whipple, K. X., and G. E. Tucker (1999), Dynamics of the stream-power river incision model: Implications for height limits of mountain ranges, landscape response timescales, and research needs, *J. Geophys. Res.*, *104*(B8), 17,661–17,674.

Whipple, K. X., E. Kirby, and S. H. Brocklehurst (1999), Geomorphic limits to climate-induced increases in topographic relief, *Nature*, *401*, 39–43.

Whipple, K. X., R. S. Anderson, and G. S. Dick (2000), River incision into bedrock: Mechanics and relative efficacy of plucking, abrasion, and cavitation, *Geol. Soc. Am. Bull.*, *112*, 490–503.

Willgoose, G. (1994), A statistic for testing the elevation characteristics of landscape simulation models, *J. Geophys. Res.*, *99*(B7), 13,987–13,996.

Willgoose, G., R. L. Bras, and I. Rodríguez-Iturbe (1991), Results from a new model of river basin evolution, *Earth Surf. Processes Landforms*, *16*, 237–254.

Zhang, P., P. Molnar, and W. R. Downs (2001), Increased sedimentation rates and grain sizes 2–4 Myr ago due to the influence of climate change on erosion rates, *Nature*, *410*, 891–897.

————————————

P. Davy and D. Lague, Géosciences Rennes, UMR 6118, CNRS, Université de Rennes I, Campus de Beaulieu, F-35042 Rennes Cedex, France. (dimitri.lague@univ-rennes1.fr)

N. Hovius, Department of Earth Sciences, University of Cambridge, Downing Street, Cambridge CB2 3EQ, UK.